nature materials

ARTICLES

PUBLISHED ONLINE: 10 AUGUST 2014 | DOI: 10.1038/NMAT4041

Stable lithium electrodeposition in liquid and nanoporous solid electrolytes

Yingying Lu[1†], Zhengyuan Tu[2†] and Lynden A. Archer[1*]

Rechargeable lithium, sodium and aluminium metal-based batteries are among the most versatile platforms for high-energy, cost-effective electrochemical energy storage. Non-uniform metal deposition and dendrite formation on the negative electrode during repeated cycles of charge and discharge are major hurdles to commercialization of energy-storage devices based on each of these chemistries. A long-held view is that unstable electrodeposition is a consequence of inherent characteristics of these metals and their inability to form uniform electrodeposits on surfaces with inevitable defects. We report on electrodeposition of lithium in simple liquid electrolytes and in nanoporous solids infused with liquid electrolytes. We find that simple liquid electrolytes reinforced with halogenated salt blends exhibit stable long-term cycling at room temperature, often with no signs of deposition instabilities over hundreds of cycles of charge and discharge and thousands of operating hours. We rationalize these observations with the help of surface energy data for the electrolyte/lithium interface and impedance analysis of the interface during different stages of cell operation. Our findings provide support for an important recent theoretical prediction that the surface mobility of lithium is significantly enhanced in the presence of lithium halide salts. Our results also show that a high electrolyte modulus is unnecessary for stable electrodeposition of lithium.

High energy and safe electrochemical storage are critical components in multiple emerging fields of technology where portability is a requirement for performance and large-scale deployment. From advanced robotics, autonomous aircraft, to hybrid electric vehicles, the number of technologies demanding advanced electrochemical storage solutions is rising. The rechargeable lithium ion battery (LIB) has received considerable attention because of its high operating voltages, low internal resistance and minimal memory effects[1–7]. Unfortunately, LIBs are now operating close to their theoretical performance limits due to the relatively low capacity of the anode (LiC_6) and the lithiated cathode materials ($LiCoO_2$ and $LiFePO_4$) in widespread commercial use. It has long been understood that a rechargeable lithium metal battery (LMB), which eschewed the use of a carbon host at the anode, can lead to as much as a tenfold improvement in anode storage capacity (from 360 mAh g^{-1} to 3,860 mAh g^{-1}) and would open up opportunities for high-energy un-lithiated cathode materials such as sulphur and oxygen, among others[8–10]. Together, these advances would lead to rechargeable batteries with step-change improvements in storage capacity relative to today's state-of-the-art LIBs.

A grand challenge in the field concerns the development of electrolytes, electrode, and battery system configurations that prevent uneven electrodeposition of lithium and other metal anodes, and thereby eliminate dendrites at the nucleation step[1]. It is understood that without significant breakthroughs in this area, the promise of LMBs, as well as of storage platforms based on more earth abundant metals such as Na and Al metal cannot be realized. Specifically, after repeated cycles of charge and discharge, growing metal dendrites can bridge the inter-electrode space, producing internal short circuits in the cell. In a volatile electrolyte, ohmic heat generated by these shorts may lead to thermal runaway and catastrophic cell failure, which places obvious safety and performance limitations on the cells. The ohmic heat generated during a short circuit may also locally melt dendrites to create regions of 'orphaned' or electrically disconnected metal that result in a steady decrease in storage capacity as a battery is cycled. LIBs are designed to remove these risks by hosting the lithium in a conductive carbon host at the anode. However, the small potential difference that separates lithium insertion into versus plating onto carbon can potentially lead to similar failure modes in an overcharged or too quickly charged LIB. Thus, the need for materials that prevent non-uniform electrodeposition of metals such as Li is also implicit in new fast-charging LIB technology targeted for electric-drive vehicles.

Researchers have for decades considered many strategies to stabilize lithium electrodeposition on metallic anodes[11–25]. Of these approaches, all solid-state batteries based on solid, ceramic electrolytes are considered by far the most promising, both from the perspective of their inherent safety and from theory[19], which indicate that a ceramic electrolyte with modulus above the shear modulus of the metallic anode can prevent dendrites from crossing the inter-electrode space. A persistent, vexing problem with ceramic electrolytes is that their room-temperature ionic conductivity rarely reach levels commonplace in liquid electrolytes and required for normal battery operation. This problem can to some extent be managed by reducing the thickness of the solid electrolyte or by operating the batteries at elevated temperature. However, these changes reveal other, more serious shortcomings, which have been most clearly demonstrated in studies of high-temperature sodium metal cells[26,27]. In these cells it was found that even at temperatures where the sodium anode is a low-modulus liquid and a high-modulus, solid sodium-beta-alumina ceramic is used as the electrolyte, metal dendrites form at the electrode/electrolyte interface and ultimately proliferate through stress and corrosion-induced cracks in the ceramic. A more recent study[14] suggests that the need for high operating temperatures can be removed by making use of nanoporous ceramics that host a low-volatility and electrochemically stable liquid electrolyte in the pores. There it is reported that these electrolytes provide a combination of solid-like mechanical modulus and liquid-like bulk and interfacial

[1]School of Chemical and Biomolecular Engineering, Cornell University, Ithaca, New York 14853-5201, USA, [2]Department of Materials Science and Engineering, Cornell University, Ithaca, New York 14853-5201, USA. †These authors contributed equally to this work. *e-mail: laa25@cornell.edu

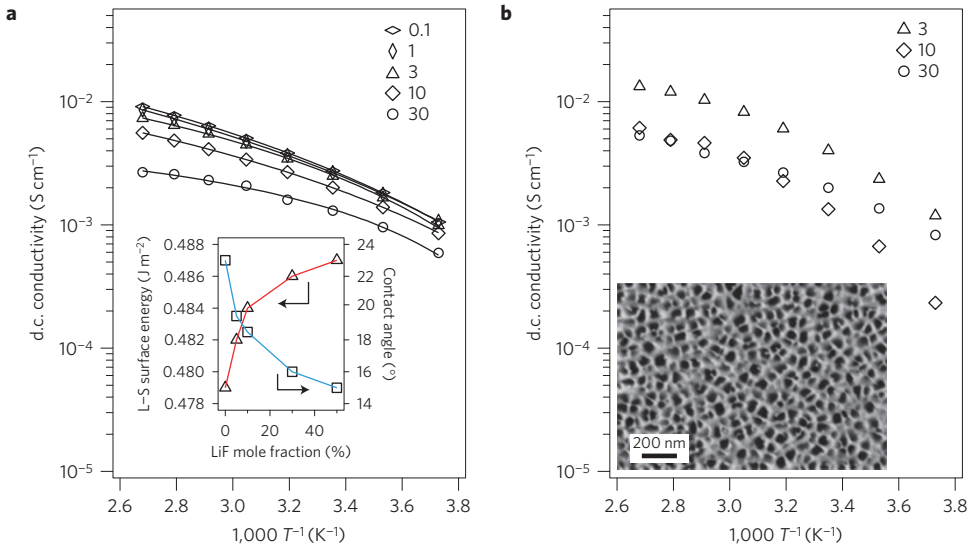

Figure 1 | d.c. ionic conductivity of 1 M ((1 − *y*) LiTFSI + *y* LiX)–PC electrolytes with various LiF mole percentages (*y* × 100%) as a function of temperature. a, Liquid electrolytes without alumina/PVDF membrane separators. The solid lines are Vogel–Fulcher–Tammann fits for the temperature-dependent ionic conductivity. The parameters used for the Vogel–Fulcher–Tammann fits are provided in Supplementary Table 2 and the cell configuration used for the measurements is shown in Supplementary Scheme 2; that is, an O-ring-shaped separator is used for the measurements. The inset shows the liquid–solid surface energy and contact angle as a function of LiF mole fraction. **b**, The same as in **a** except the electrolyte is infused into a nanoporous alumina/PVDF membrane that fills the inter-electrode space. The SEM image shows the nanopore structure of the alumina membrane with mean pore diameter around 40 nm.

conductivities at room temperature. Furthermore, when employed in LMBs, they substantially increase the lifetime of cells cycled at low and moderate current densities, but post-mortem inspection of the surface of the porous ceramic host reveals that, as in the case of the bulk ceramics, dendrites are still able to nucleate and proliferate on the surface, but seem unable to penetrate through the pores of the porous material.

A long-standing puzzle in the field is that secondary batteries based on some metals (for example, Mg) show no evidence of electrode instability and dendrite formation under deposition conditions where dendrites form and proliferate in others, such as Li (ref. 28). At low surface deposition rates, thermodynamic and surface forces determine whether electrodeposited atoms preferentially form the low-dimensionality, fibre-like structures that lead to dendrites, or whether they form higher-dimensional crystalline phases. In contrast, at the intermediate and high surface deposition rates common in batteries, the mobility of atoms at the interface determines whether smooth or rough electrodeposits are created. Density functional theoretical analysis of Mg and Li electrodeposits at a vacuum/metal interface reveals that Mg–Mg bonds are on average 0.18 eV stronger compared with a Li–Li bond[29]. This means that under the same deposition conditions, the probability of a lower-dimension, fibre-like Mg deposit spontaneously transforming to a higher-dimension crystal is more than 1,000 times higher than that for the corresponding transition in lithium. In electrolytes, these differences are only slightly altered by the interfacial tension, which is orders of magnitude lower, perhaps explaining why Li surfaces are more prone to nucleate dendrites irrespective of the electrolyte. A surprising and heretofore unexplored prediction from recent joint density functional theoretical (JDFT) calculations[30,31] is that the presence of halide anions, particularly fluorides, in an electrolyte produces as much as a 0.13 eV reduction in the activation energy barrier for Li diffusion at an electrolyte/lithium metal electrode interface. If correct, this means that it should be possible to increase the surface diffusivity by more than two orders of magnitude, which may lead to large improvements in the stability of Li electrodeposition and dendrite suppression in simple liquid electrolytes.

We herein report on the stability of lithium electrodeposition in common liquid electrolytes reinforced with halogenated lithium salts. Remarkably, we find that consistent with expectations from the JDFT calculations, premature cell failure by dendrite growth and proliferation can be essentially eliminated in plate-strip type experiments even at high operating current densities. In more aggressive, high-rate polarization experiments, we find levels of dendrite suppression in room-temperature liquid electrolytes that are either comparable to or superior to all previous reports from elevated-temperature studies of polymer[18,32] and other solid-state electrolytes long thought to be essential for developing reliable LMBs. Experimental characterization of the interfacial tension and impedance at the electrolyte/lithium metal interface confirm that the interfacial mobility is a strong decreasing function of halogenated lithium salt and is the most likely source of the improved stability of Li electrodeposits in liquids.

Electrolytes containing 1 M Li cations were studied in two configurations: in liquid form; and as liquids infused in nanoporous solids. Electrolytes employed in both situations were created by blending predetermined amounts of halogenated lithium salts and lithium bis(trifluoromethanesulphonyl)imide (LiTFSI) in a low-volatility propylene carbonate (PC) liquid host. For simplicity, this study focuses on electrolytes of the form 1 M ($(1-y)$ LiTFSI + y LiX) in PC, where y is the mole fraction of LiX (X = F, Cl, Br, I) in the electrolyte. A key assumption in the analysis of refs 30,31 is that the halogenated salt additive deposits to form a crystalline film (SEI) conformal with the lithium metal anode. Salt additives such as LiF that are poorly soluble in PC at room temperature[33] may produce SEI layers that approximate the situation imagined in the theory; complementary studies employing salt additives such as LiBr with greater solubility in PC allow us to test the robustness of the stabilization provided by such additives in more typical cases where a disordered, heterogeneous SEI is formed. To explore the consequences of our observations on the lifetime of lithium metal batteries, we also performed a small number of studies using

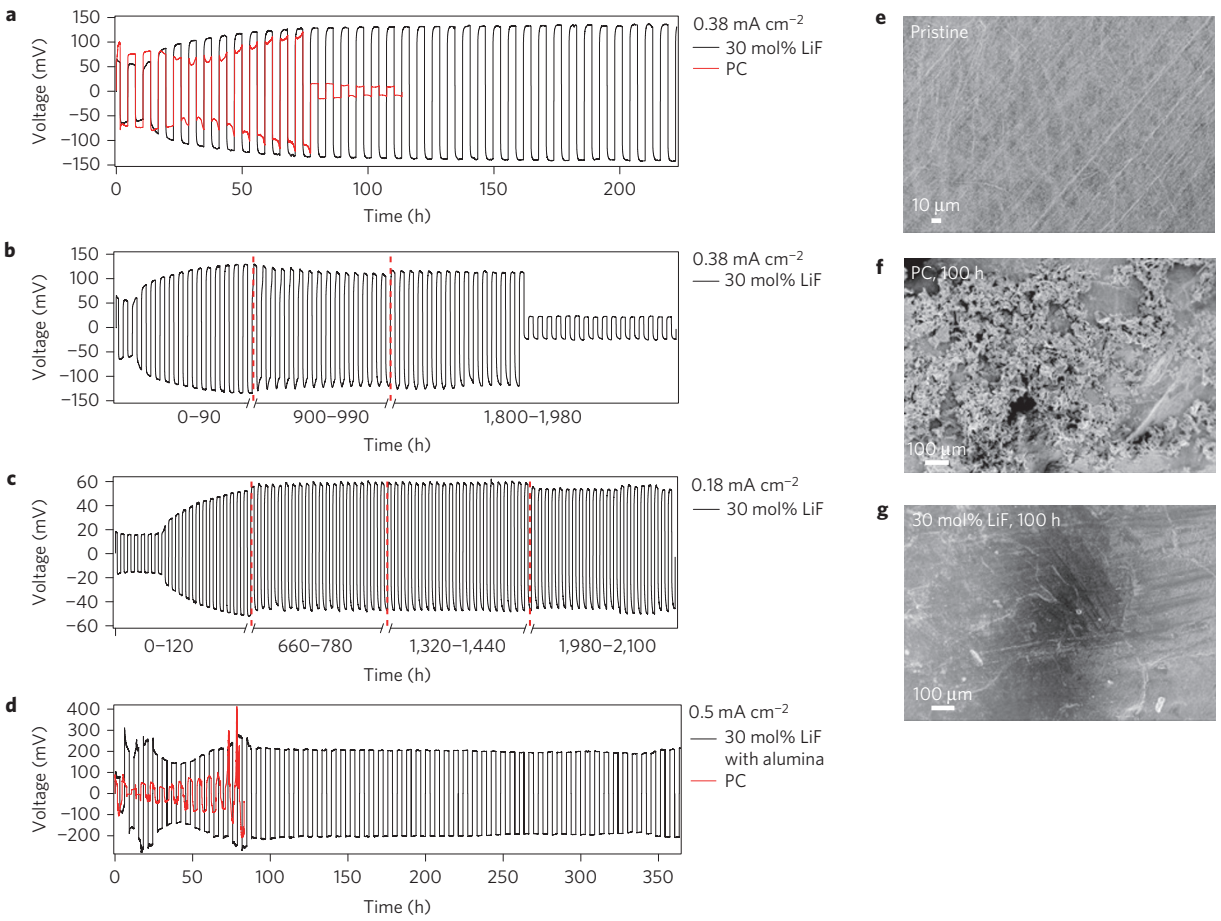

Figure 2 | Voltage versus time for a symmetric lithium cell where each half-cycle lasts 3 h. a, Initial voltage profiles for 1 M ((1−*y*) LiTFSI + *y* LiF)–PC with $y=0.3$ (black) and $y=0$ (red) at a fixed current density of 0.38 mA cm^{-2}. **b**, Extended time voltage response of the electrolyte in **a** with $y=0.3$ at a current density of 0.38 mA cm^{-2}. **c**, Typical time-dependent voltage for 1 M ((1−*y*) LiTFSI + *y* LiF)–PC electrolyte with $y=0.3$ at a current density of 0.18 mA cm^{-2}. Broken linear time axes are used in **b**,**c** to present data over an extended period of time. The red vertical lines identify positions of the time axis breaks. **d**, Initial voltage profiles for 1 M ((1−*y*) LiTFSI + *y* LiF)–PC with $y=0.3$ (black) and $y=0$ (red) in cells using nanoporous alumina/PVDF membrane separators at a current density of 0.50 mA cm^{-2}. The initial voltage disturbance is due to the electrolyte consumption and SEI layer formation. The voltage reaches a stable plateau after 80 h and lasts for over 350 h. Such stable performance at high current density seems to originate from two factors: the LiF additive stabilizes the lithium deposition; the high conductivity and modulus of the nanoporous alumina separator facilitates straightforward cell assembly and prevents proliferation in the inter-electrode space of any dendrites that do form. **e**–**g**, SEM analyses. **e**, Pristine lithium anode before galvanostatic cycling. **f**, Lithium anode in contact with 1 M ((1−*y*) LiTFSI + *y* LiF)–PC with $y=0$ after 100 h cycling at 0.38 mA cm^{-2}. **g**, Lithium anode in contact with 1 M ((1−*y*) LiTFSI + *y* LiF)–PC with $y=0.3$ after 100 h cycling at 0.38 mA cm^{-2}.

blends of lithium fluoride (LiF) and lithium hexafluorophosphate ($LiPF_6$) in a 50:50 blend of ethylene carbonate (EC) and diethylene carbonate (EC:DEC). As the most impressive enhancements in interfacial mobility predicted by JDFT are for electrolytes containing LiF, this first communication will focus on these materials. Figure 1a reports the ionic conductivity for the 1 M ($(1-y)$ LiTFSI + y LiX)–PC electrolytes as a function of mole percentage ($y \times 100\%$) of LiF salt in the electrolytes and temperature. It is apparent that for $y \leq 0.03$, conductivities essentially identical to the measured values for a LiTFSI–PC liquid electrolyte control[12] are found. At LiF concentrations above 3 mol%, the conductivity falls with increasing LiF content and the shape of the conductivity-versus-temperature profiles are seen to become flatter, meaning that the apparent activation energy barrier for ion transport is lower (Supplementary Table 2). For $y=0.1$, the electrolyte conductivity is reduced by around 23% and at $y=0.3$ it is 1.3 mS cm^{-1} (more than three orders of magnitude higher than the measured conductivity of the 'soggy-sand' electrolyte obtained when $y=1$ (Supplementary Table 2)). A lower bulk electrolyte ionic conductivity on addition of LiF is consistent with expectations based on the reduced dissociation of the salt, relative to LiTFSI, and consequent lower population of mobile ions in solution. It is also expected from the salt dilution effect anticipated on addition of the poorly soluble LiF salt additive to PC. The inset to the figure shows the effect of LiF on the wettability/contact angle (right axis) and surface energy (left axis) of the electrolyte with a lithium metal surface (Supplementary Fig. 1 and Table 1). The measurements were performed using a contact angle goniometer with the lithium sample enclosed in a home-made argon-filled chamber. It is apparent from the figure that addition of LiF causes a non-monotonic decrease in contact angle and a commensurate rise in interfacial energy. A recent stability analysis for lithium deposition predicts a weak, inverse relationship between the growth rate κ_{mu} of the most unstable electrodeposition modes and surface energy γ of the form, $\kappa_{mu} \propto 1/\sqrt{\gamma}$ (ref. 34). This means that the modest enhancements in surface energy created in electrolytes by increasing y are, alone, not expected to lead to pronounced changes in dendrite growth rates. Later, we will also show that electrodeposition of lithium metal in these electrolytes produce isolated mushroom-like structures of diameter around 40 μm. The increase in surface energy produced on addition of LiF

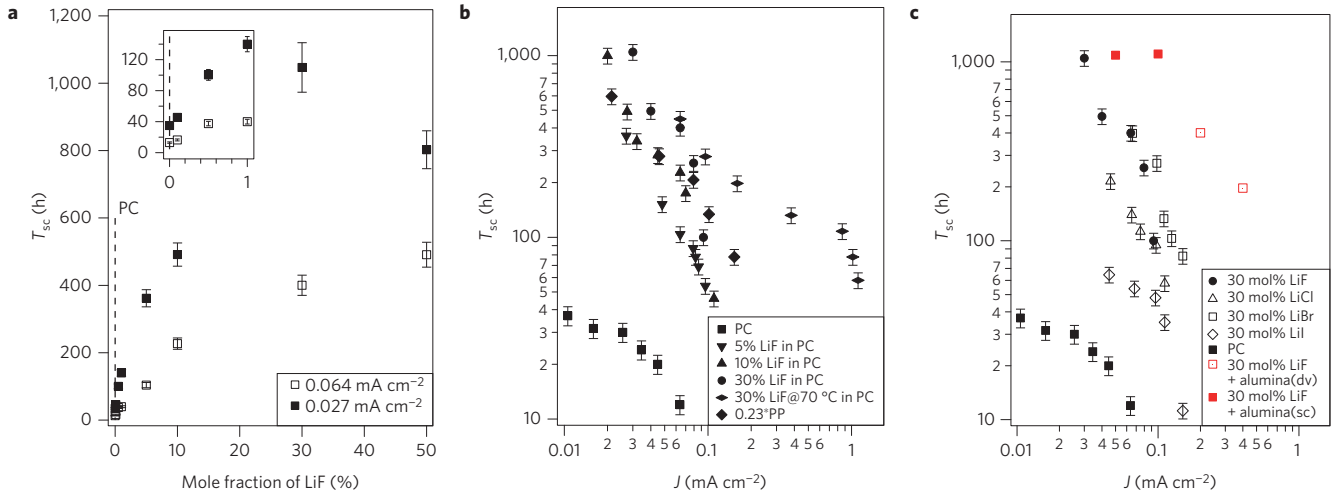

Figure 3 | Short-circuit time T_{sc} from galvanostatic polarization measurements for symmetric lithium cells. a, T_{sc} as a function of LiF mole percentage at 0.027 mA cm^{-2}, 0.064 mA cm^{-2}. **b**, T_{sc} as a function of current density J for various LiF concentrations and for PP TFSI. **c**, T_{sc} as a function of current density J for 1 M ((1−y) LiTFSI +y LiX)–PC with y = 0.3 and X = F, Cl, Br and I. The red markers are used to represent results for cells based on nanoporous alumina/PVDF membranes infused with 1 M ((1−y) LiTFSI +y LiF)–PC electrolytes. The error bars are standard deviations about the mean values obtained from six independent measurements performed under the same cell running conditions. The filled red symbols indicate the cells that short-circuit; the open red symbols represent the ones in which the voltage diverges instead of shorts; post-mortem analysis of the Li metal source electrode shows that the material is completely consumed, indicating that the cells run dendrite-free for the entire assessment period. Measurements were all conducted at room temperature unless noted otherwise.

to the electrolytes is therefore many orders of magnitude lower than the differences in bonding energy between Mg–Mg and Li–Li atoms to significantly change the tendency of Li to form lower-dimensional dendritic structures.

Figure 1b reports the d.c. conductivity for nanoporous solid electrolytes created by infusing 1 M ((1−y) LiTFSI +y LiX)–PC electrolytes into nanoporous Al_2O_3/PVDF monoliths (see lower inset) with a nominal pore diameter of 40 nm. The detailed preparation protocols for these electrolytes are provided in the Supplementary Information. It is apparent from Fig. 1b that although the effect of LiF composition on conductivity is more complex than for the liquid electrolytes, over the range of LiF compositions studied the electrolytes again exhibit room-temperature conductivities above 10^{-3} S cm^{-1}; underscoring their suitability as room-temperature electrolytes for lithium batteries. Electrochemical stability of LiF-containing electrolytes was characterized by cyclic voltammetry and the results are reported in Supplementary Fig. 2. With 30 mol% LiF, the width of the electrochemical stability window is observed to increase measurably. The peak in the voltammogram at around 4.1 V versus Li/Li$^+$ in the first cycle is in fact consistent with formation of a passivation film on the electrode that protects the electrode from further reaction with the electrolyte. Later we will employ a variety of tools to study the composition of this layer under static and electrochemical conditions and will see that it is primarily comprised of LiF.

We investigated electrodeposition of Li in the liquid and nanoporous LiF + LiTFSI–PC-based electrolytes using galvanostatic cycling of Li|1 M ((1−y) LiTFSI +y LiF)–PC|Li symmetric lithium cells in which the lithium striping/plating process is cycled over three-hour charge and discharge intervals under fixed currents designed to mimic operation in a LMB. The cells are configured to ensure that during each three-hour period sufficient lithium is transported between electrodes to create a dendrite bridge in the inter-electrode space to short-circuit the cells. The cells also do not include a separator and, once formed, the only resistance to dendrites bridging the inter-electrode spacing is provided by the intervening liquid electrolyte. Figure 2a compares the voltage profiles observed in symmetric cells containing electrolytes with and without LiF at a fixed, high current density of 0.38 mA cm^{-2}.

The figure shows that cells that do not contain LiF in the electrolyte exhibit a large and irreversible drop in voltage consistent with catastrophic failure by a dendrite-induced short circuit, in as little as 75 h of operation (that is, less than 13 cycles of charge and discharge). In contrast, cells containing 30 mol% LiF in the electrolyte cycle stably for more than 1,800 h (300 cycles of charge and discharge) before succumbing to failure in the same manner. This nearly 25-fold enhancement in cell lifetime achieved on addition of LiF to a liquid electrolyte is considerably higher than any previous report for cells in which solid polymers[18], composites[12,13,15] and other mechanical agents are used to protect lithium metal electrodes against premature failure by dendrite-induced shorts. It is also unexpected on the basis of any of the current continuum theories[19,23,24,34], for electrodeposition of Li. Our findings are even more significant because the current experiments are performed at room temperature and at substantially higher current densities than those typically used for evaluating solid polymer or ceramic electrolytes. Figure 2c reports voltage profiles for cycling experiments performed at comparable current densities as in previous studies using polymers and other mechanical agents. Remarkably, even after 2,100 h of continuous operation, the cell shows no evidence of failure. Figure 2d reports a similar result for cells based on nanoporous membranes infused with liquid electrolytes, but cycled at a very high current density of 0.5 mA cm^{-2}. Whereas cells with the control LiTFSI–PC electrolyte are seen to quickly fail, those containing LiF in the electrolyte settle down over a period of around 75 h and cycle stably for more than 350 h.

Figure 2e–g shows scanning electron micrographs of the lithium metal electrode surface before cycling (Fig. 2e), after 100 h of cycling in a LiTFSI–PC control electrolyte (Fig. 2f), and after 100 h of cycling in a 1 M ((1−y) LiTFSI +y LiF)–PC with y = 0.3 (Fig. 2g). To facilitate the latter characterization, the lithium metal was thoroughly washed with PC to remove any electrolyte or salt residues and the electrolyte solvent was removed under vacuum. It is evident from the figure that the improved lifetimes of the cells containing LiF coincide with

the observation of virtually pristine Li metal electrodes after extended cycling.

Unidirectional galvanostatic polarization of symmetric lithium cells provides a convenient, accelerated-testing scheme for assessing the stability of lithium metal electrodes during electrodeposition. In this approach, lithium is continuously stripped from one electrode (source) and plated on the other (substrate) until the cell fails by consumption of all of the lithium or as a result of a dendrite-induced short circuit. A constant current density is applied to the cell and the corresponding voltage profile is obtained as a function of time. The time (T_{sc}) at which a sharp drop-off in the potential is observed provides an estimate for the cell lifetime. As there is no pause in the deposition, as occurs when the direction of the current is reversed in the cyclic plate-strip experiment discussed in the last section, there is no opportunity for defects produced by instability in one deposition cycle to heal before they nucleate dendrites that ultimately short-circuit the cell. Consequently, cell failure by dendrite-induced short circuits is observed on timescales as much as one order of magnitude lower than for the plate-strip cycling measurements[12,24,25].

Figure 3a reports measured T_{sc} values as a function of LiF concentration in the electrolyte at two current densities. Consistent with the observations reported in the previous section, the figure shows that increasing y in the electrolyte produces large increases in cell lifetime. The top inset shows that addition of as little as 1 mol% LiF ($y=0.01$) produces more than a threefold enhancement in cell lifetime at both low (0.027 mA cm^{-2}) and moderate (0.064 mA cm^{-2}) current densities. The figure further shows that at a higher LiF content the relationship between T_{sc} and LiF composition in the electrolyte is nonlinear. At 30 mol% LiF, it is seen that more than a 30-fold enhancement in cell lifetime is achieved at either current density, confirming the earlier observations based on cyclic plate-strip experiments. The ability of LiF salt to extend cell lifetime seems to reach its maximum level at around 30 mol% LiF. For a higher LiF mole fraction (50 mol% LiF), there is a decrease of T_{sc}, which might be attributed to a variety of factors including the low d.c. conductivity, poor solubility of LiF in PC, which may increase the thickness and resistivity of the SEI, and low mobile ion concentration in the electrolyte. It is also difficult to polarize the cell at relatively high current density for the same reason[23].

Figure 3b studies the effect of current density, J, and temperature on T_{sc} for electrolytes containing varying concentrations of LiF, including a PC electrolyte containing 23 vol% of the ionic-liquid methyl-3-propylpiperidinium (PP) TFSI known for its exceptional ability to facilitate stable electrodeposition of lithium[11,12]. It is clear from the figure that both in terms of the variation of T_{sc} with J and the enhancements in lifetime achieved relative to the electrolyte without additives, the LiF-based electrolytes with around 30 mol% LiF perform at least as well as those containing PP TFSI. As previously reported for electrolytes containing PP TFSI, T_{sc} exhibits a power-law dependence on J, $T_{sc} \sim J^{-m}$, over a wide range of current densities[13,24,25]. Power-law exponents m obtained from the data are provided in Supplementary Table 2 and show no noticeable dependence on LiF composition. It is also apparent from the figure that at 70 °C electrolytes containing LiF exhibit T_{sc} values with little sensitivity to J over a range of current densities, allowing these electrolytes to achieve 100-fold or more enhancements in cell lifetime, relative to the control electrolyte at 25 °C. Figure 3c nicely shows that LiF is not unique and that other halogenated lithium salts, especially LiBr, are able to significantly extend the lifetime of lithium metal electrodes. This result is important because unlike LiF, LiBr is readily soluble in PC. The result suggests that a uniform crystalline lithium halide salt SEI layer assumed by the theory is perhaps not necessary for achieving the lifetime improvements. Figure 3c further shows that T_{sc} values measured using nanoporous electrolytes[14] (also see Supplementary Fig. 7) containing LiF are substantially higher than those measured in any of the other systems and are virtually independent of J. The two open red symbols are results for cells where no short circuiting was observed, but in which

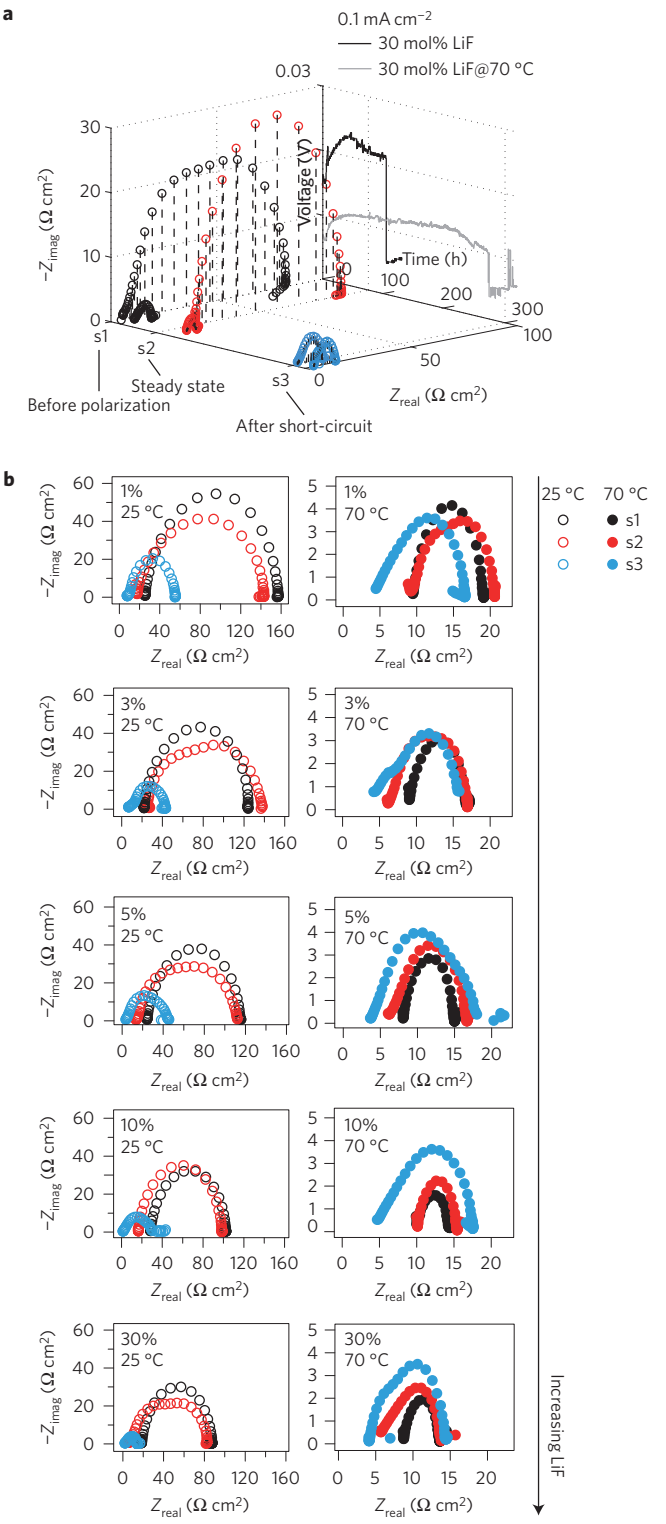

Figure 4 | Voltage profile at a fixed current density and impedance spectra of the three stages s1, s2 and s3 at 25 °C and 70 °C. a, Voltage profiles and impedance spectra at 0.1 mA cm^{-2} for 1 M ((1−y) LiTFSI + y LiX)-PC with $y=0.3$ electrolyte. **b**, Impedance spectra for 1 M ((1−y) LiTFSI + y LiX)-PC electrolytes with $y=0.01, 0.03, 0.05, 0.1$ and 0.3. The impedance spectra with alumina/PVDF separator are reported in Supplementary Fig. 8.

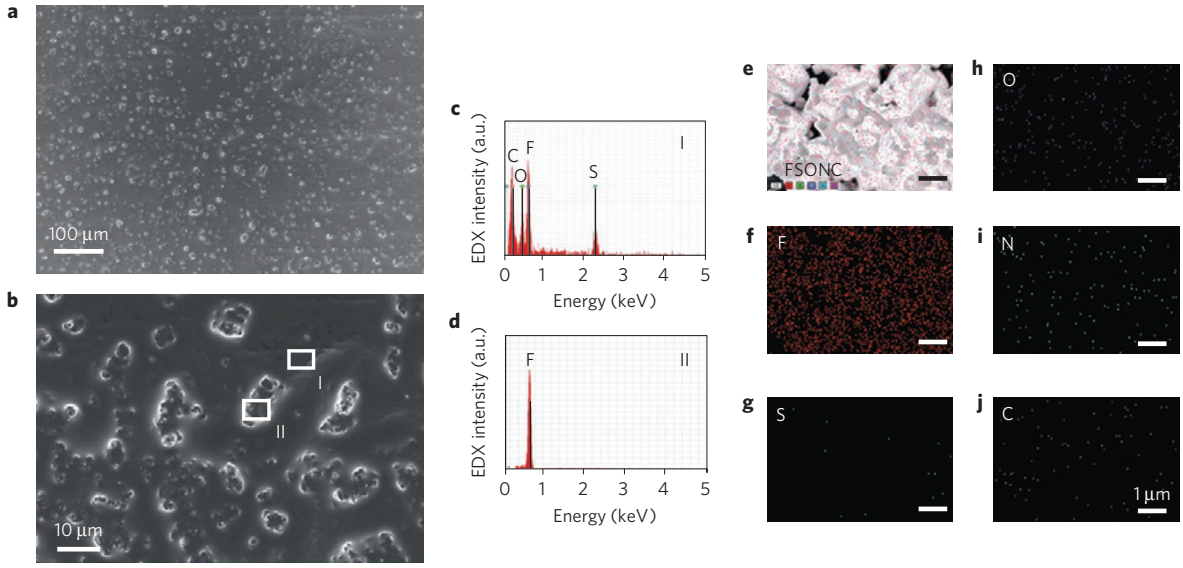

Figure 5 | The morphology and distribution of LiF clusters on lithium foil by SEM and EDX. a,**b**, SEM images of salt clusters on lithium foil at different scales. **c**,**d**, EDX spectrum of region I and II, respectively, showing that LiF forms clusters on lithium foil because of its insolubility in PC. **e**–**j**, EDX mapping of region II (**e**), showing signals of fluorine (**f**), sulphur (**g**), oxygen (**h**), nitrogen (**i**) and carbon (**j**).

the voltage diverged as a result of all of the lithium in the stripping electrode being plated on the other electrode without creating dendrite-induced short circuiting. It is remarkable that these cells show no evidence of short circuiting at high current densities normally inaccessible in galvanostatic polarization experiments in symmetric Li cells. Post-mortem scanning electron microscopy (SEM) analysis for these cells is provided in Supplementary Fig. 3.

Analysis of the electrode/electrolyte interface at different stages of polarization provides additional insight into the role played by LiF. Impedance spectroscopy is a frequency-domain technique that allows the complex resistance or impedance in all components of a cell (electrode, electrolyte, and their interfaces) to be determined as a function of temperature. Impedance spectra of the symmetric lithium cells before unidirectional galvanostatic polarization, at steady state, and after cell failure were collected and typical results are reported in Fig. 4a,b. Measurements were performed at 25 °C and 70 °C to characterize the effect of temperature. It is readily apparent from the figure that the interfacial impedance (related to the width of the curves) drops noticeably at the point of short circuiting. Note that it is not possible to fit the impedance spectra by an equivalent circuit model because the surface is no longer uniform once the dendrite starts to form. Figure 4a compares the impedances of the three stages for 30 mol% LiF + LiTFSI–PC electrolyte at 25 °C and 70 °C. Both the bulk (related to the lower intercept of the spectra) and interfacial impedances decrease sharply with only a 45 °C temperature increase.

Figure 4b shows the impedance spectra for the 1 M $((1-y)$ LiTFSI $+y$ LiX)–PC electrolytes containing 1, 3, 5, 10 and 30 mol% LiF. At 25 °C, the bulk and interfacial impedances are seen to change slightly after the onset of polarization, but as already noted drop substantially after the cell short-circuits. Electrolytes with higher LiF mole fraction have comparable bulk, but measurably lower interfacial impedances at all stages. This suggests that LiF has the ability to selectively enhance Li^+ ion transport near the electrode/electrolyte interface. When operating at 70 °C, spectra at all three stages exhibit similar bulk and interfacial impedances between 5 and 15 $\Omega\,cm^2$ with negligible dependence of the LiF composition of the electrolyte. It is significant that these conditions produce cells that exhibit the longest lifetimes at the highest current densities studied. In general, the lowered impedance created by LiF seems to lead to the large extension of cell lifetimes observed, and the sharply reduced impedance with temperature explains the tremendous enhancement of cell lifetime at high temperature in terms of faster lithium ion migration in the SEI, which facilitates stable deposition. We believe this result nicely underscores that the mechanism by which LiF acts is primarily by lowering the interfacial resistance.

If LiF stabilizes electrodeposition by enhancing interfacial transport of Li^+ ions, knowledge of the morphology and chemical make-up of the SEI formed on the lithium metal surface is important. We employed a combination of SEM, energy dispersive X-ray analysis (EDX), and X-ray photoelectron spectroscopy (XPS) with depth profiling analysis to study the surface of lithium anodes prepared under static (no electrochemical cycling) and dynamic (after cycling) conditions. The lithium metal electrodes used for these studies were harvested from coin cells in an argon-filled glovebox and dried under vacuum in the glovebox; they were not washed with PC as in the case of the electrodes used for the post-mortem SEM analysis in Fig. 2. Figure 5a,b and Supplementary Fig. 9 show that at most LiF concentrations studied, there are microcrystalline structures on the surface of the Li metal electrode. As the electrolyte in all cases is 1 M $((1-y)$ LiTFSI $+y$ LiX), chemical analysis of the surface deposits provides indirect but meaningful insights into the electrode/electrolyte interface during cell operation. The concentration of these deposits, for example, is seen to clearly increase with y (Supplementary Fig. 9a,b) and the size and shapes are very different for electrolytes in which LiF is the only salt. Supplementary Fig. 9d further shows that in traversing the halogen series from F to I, both the size and areal density decrease, with the surface of Li metal electrodes harvested from electrolytes containing soluble salt additives such as LiI and LiBr showing almost no signs of the microcrystallites that dominate the surface landscape when LiF is used.

Survey and single-element composition analysis of the electrode surface by EDX (Fig. 5c–j) indicates that the deposits on the electrode are fluorine rich and, on the basis of the absence of other elements detectable by EDX, that they are most likely LiF. By employing XPS in tandem with inert gas ion sputtering/etching, a compositional depth profile can be generated. Analysis of the XPS binding energy profiles (Supplementary Fig. 10), particularly

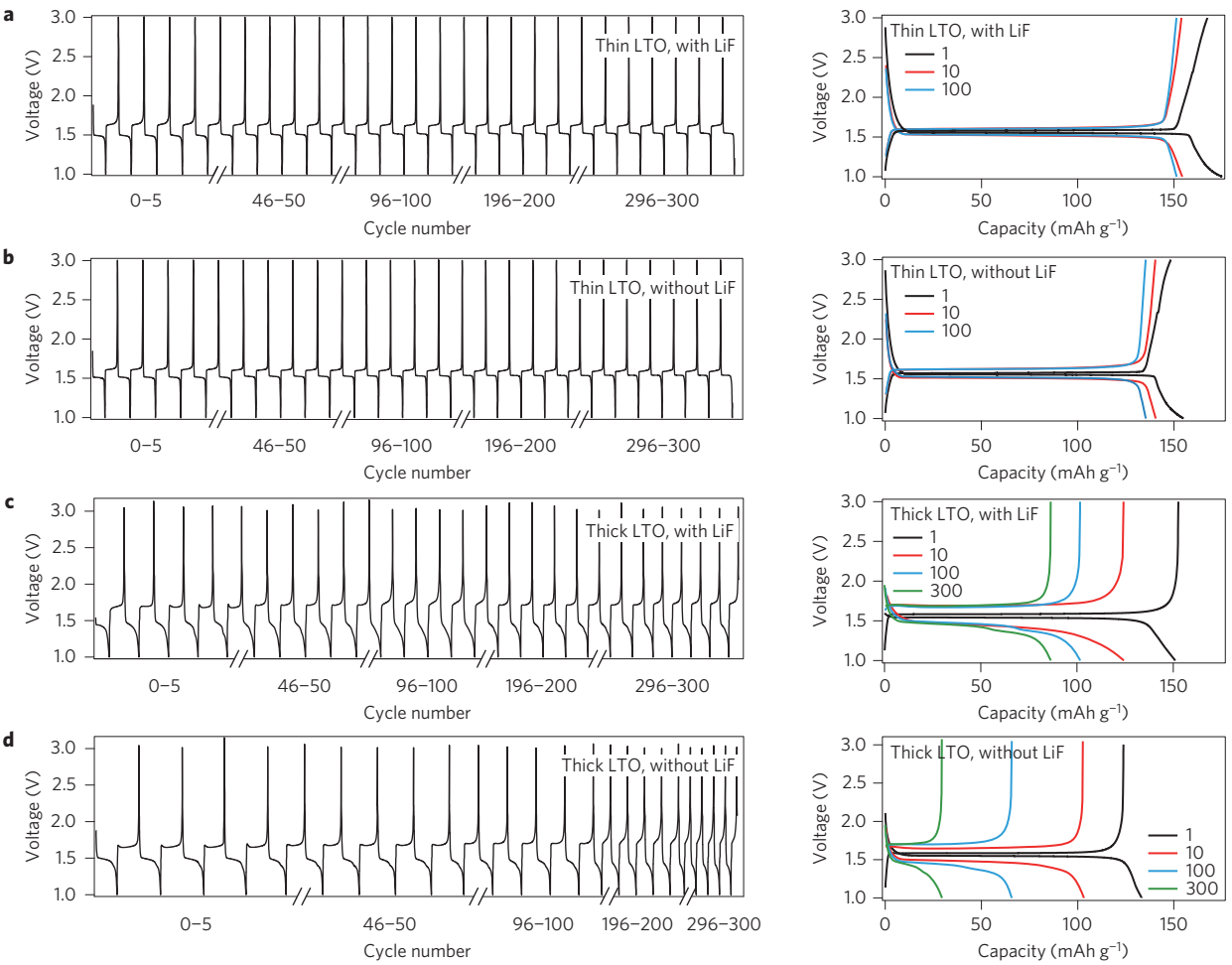

Figure 6 | Charge–discharge characteristics of $Li/Li_4Ti_5O_{12}$ (Li/LTO) with 30 mol% LiF + LiTFSI/EC:DEC and LiTFSI/EC:DEC electrolytes at room temperature. a,**b**, For the thin LTO electrode: voltage versus time profile for the first 5 cycles, 46–50 cycles, 96–100 cycles, 196–200 cycles and 296–300 cycles at 1 C rate (0.18 mA cm^{-2}) with LiF (**a** left) and without LiF (**b** left). About 0.88 μm lithium (charge passed = 0.65 C cm^{-2}, about 2.2 μm LTO is reacted) is transported from one electrode to the other in each half-cycle. Initial, 10th, 100th charge–discharge profiles with LiF (**a** right) and without LiF (**b** right). **c**,**d**, For the thick LTO electrode: voltage versus time profile for the first 5 cycles, 46–50 cycles, 96–100 cycles, 196–200 cycles and 296–300 cycles at 1C rate (2 mA cm^{-2}) with LiF (**c** left) and without LiF (**d** left). About 9.8 μm lithium (charge passed = 7.2 C cm^{-2}, about 24.5 μm LTO is reacted) is transported from one electrode to the other in each half cycle. Initial, 10th, 100th, 300th charge–discharge profiles with LiF (**c** right) and without LiF (**d** right).

those associated with fluorine, reveals a single dominant peak centred near 685 eV for all but the first layer where the peak is downshifted to 690 eV. Supplementary Fig. 10b indicates that even after electrochemical measurements suggest that the cells have short-circuited and that dendrites have crossed the inter-electrode space, the XPS profile at all but the first layer shows a single dominant fluorine peak near 685 eV. Fluorine atoms bonded to Li are recognizable by their 685–686 eV (ref. 35) binding energy, meaning that down to a distance of at least 140 nm from the interface, LiF is the dominant species on the lithium metal surface. The downshift centred at 690 eV is most likely caused by the LiTFSI overlayer[35,36] visible in the EDX measurements (Fig. 5c) from the smoother surface regions. Analysis of the binding energy associated with lithium reveals a more complex picture of the surface landscape (Supplementary Fig. 10b,c). Before polarization, the lithium signals on the first few layers exhibit binding energies near 56 eV, which indicates the existence of LiF (refs 35,36). The downshifting of lithium peaks to 54–55 eV on deeper layers indicates that LiOH and Li_2CO_3 (ref. 37) are the dominant species present as one moves away from the interface. Significantly, after the cell short-circuits, the lithium peaks are seen to be quite different. An obvious peak downshifting is observed starting from the second layer to the fifth layer, and the binding energies of peaks on deeper layers slightly increase. The first downshifting can be explained in terms of either a Li_2O or metallic lithium species present in an overlayer near the electrode/electrolyte interface, whereas the upshifting at deeper depths can be explained either in terms of the existence of LiOH or Li_2CO_3 at deeper layers. Taken together, these results therefore suggest that the lower interfacial impedance apparent in electrolytes containing LiF is a result of the selective enrichment of LiF at the interface. We suspect that even the more soluble LiBr extends electrode lifetime by a similar mechanism; more extensive experiments with electrolytes containing this salt are underway to establish whether the same processes govern performance of LiBr.

To further evaluate the suitability of electrolytes containing LiF salts in LMBs, a more commonly used electrolyte blend comprised 1:1 (v:v) EC:DEC with and without LiF was investigated at room temperature using a $Li/Li_4Ti_5O_{12}$ (LTO) half-cell. Previous studies show that the LiF is around 40,000 times more soluble in EC than in PC at 40 °C (ref. 33). The half-cell studies therefore provide a complement to the previously discussed polarization studies using more soluble LiBr and LiCl salt additives in PC.

LTO is also a zero-strain electrode material under development for commercial use in electric vehicles and is capable of cycling at both low and high rates for consecutive charge and discharges[38]. In practice, even commercial LTO spinel powder yields a well-defined discharge plateau at 1.55 V in carbonate electrolytes, and a discharge capacity close to the theoretical capacities (175 mAh g^{-1}) when accommodating lithium and negligible round-trip IR losses[39]. To characterize the effect of LiF on the performance of a Li/LTO half-cell, thin LTO (15 μm of active material) and thick LTO (64 μm of the active material) were studied in an accelerated procedure employing a very high current density of 2.0 mA cm^{-2} (1 C). For cells based on the thick LTO electrode, an activation process at 0.1 C for 10 cycles was employed before the higher current density experiments. A two-hour charge/discharge protocol allows enough lithium to be transported during each cycle to create dendrites that are large enough to short-circuit the cells based on the thick electrode, whereas those based on the more common thin electrodes do not allow sufficient lithium transport to create a dendrite that spans the inter-electrode space.

Figure 6a,b (left panels) shows the voltage profiles obtained using the thin electrodes with and without LiF additive. Unlike the symmetric cells where the current is fixed and the voltage is left unconstrained, the voltage range and current are fixed in these experiments. The onset of failure as a result of formation of dendrite shorts or regions of disconnected lithium is then expected to show up in the lifetime or capacity of the cells. It is apparent from Fig. 6a (left) that addition of LiF to the electrolytes increases the discharge capacity, but otherwise does not alter the cycling performance of the cells. The blow-up charge and discharge curves in Fig. 6a,b (right panels) show that the round-trip IR losses in both cells are quite minimal, as expected for LTO. The corresponding results for the thick electrodes are reported in Fig. 6c,d. It is apparent from the voltage profiles in Fig. 6c,d (left panels) that a small change in the LiF-containing electrolytes not only increases the accessible discharge capacity, but substantially improves the cycling stability of the cells. This latter feature is consistent with what one might expect from the earlier observations based on symmetric Li–Li cells that show that LiF improves the stability of electrodeposition.

In summary, motivated by recent JDFT calculations, which show that the presence of lithium halides, particularly LiF, at an electrolyte/lithium metal interface should yield large improvements in stability of Li electrodeposition, we studied physical and electrochemical properties of electrolytes containing lithium halide salts as additives. Consistent with expectations from the theoretical predictions, we report that simple addition of halogenated lithium salts to a conventional low-mechanical-modulus liquid electrolyte such as PC leads to marked stabilization of electrodeposition at a lithium electrode and commensurate improvements in the lifetime of lithium batteries using metallic lithium as the anode. In plate-strip symmetric cell studies, we find that Li–Li symmetric cells employing the Li halide salt-reinforced electrolytes and cycled under similar conditions as reported for solid polymer and ceramic electrolytes, except at room temperature, exhibit no evidence of short circuiting. In more aggressive polarization studies, we find that infusing the electrolytes in the pores of a nanoporous ceramic leads to much larger cell lifetimes than any previously reported room-temperature LMB. Our findings seem significant for at least three reasons. First, they demonstrate that the popular assumption inspired by intuition and supported by continuum modelling, that a high mechanical modulus is a requirement for an electrolyte that can stop growth and proliferation of lithium dendrites, is not generally correct. Second, electrolyte reinforcement by lithium halide salts provides an inexpensive, easy-to-use strategy for stabilizing electrodeposition of lithium metal that promises to enable technological and scientific advances in the field. Third, our findings underscore the benefits of density functional and other atomistic simulation approaches for guiding new materials designs for high-energy batteries.

Methods

Predetermined quantities of lithium halide salts (LiF, LiCl, LiBr, LiI) and LiTFSI or $LiPF_6$ were dissolved in PC and EC:DEC (1:1 (v:v) EC:DEC) electrolyte mixtures. The total lithium salt concentration in the electrolytes was kept constant at 1 M. All materials used in the study, LiTFSI, $LiPF_6$, LiF, PC, EC and DEC, were dried rigorously using a previously reported method[12,13,40] (also see Supplementary Information).

Composite nanoporous alumina membranes were prepared using our previously reported approach[14]. Briefly, nanoporous alumina membranes were soaked in polyvinylidene fluoride hexafluoropropylene (PVDF-HFP)/DMF solution. A phase separation approach was adopted to prepare sandwich-type alumina/PVDF-HFP membranes. These membranes were immersed in 1 M $((1-y)$ LiTFSI $+y$ LiF)–PC electrolytes with $y=0.3$ for at least 24 h before their use to facilitate complete infiltration of the liquid electrolyte into the nanoporous membrane. Electrochemical measurements were performed in the coin cell configuration depicted in Supplementary Scheme 1.

The thinner LTO electrodes used were comprised of 80% of LTO, 10% of carbon black, and 10% of PVDF binder. A predetermined amount of *N*-methylpyrrolidone was added as solvent and the resultant slurry was thoroughly mixed. A doctor blade was used to coat the slurry onto a clean copper sheet and the coating was rigorously dried under vacuum. The thicker LTO electrodes (64 μm in thickness) used in the half-cell battery experiments were provided by the US Department of Energy's (DOE) Cell Fabrication Facility, Argonne National Laboratory and used as received.

Symmetric lithium metal coin cells (2032 type, Supplementary Scheme 2) were used for dielectric spectroscopy, impedance spectroscopy, cyclic voltammetry, and for galvanostatic polarization and cycling measurements. Ionic conductivities were measured using a Novocontrol N40 broadband dielectric spectrometer. The galvanostatic polarization and cycling measurements were conducted using a Neware CT-3008 battery tester. Impedance spectra were measured as a function of frequency in a step heating procedure using an impedance spectrometer. For post-mortem studies, cells were disassembled in an argon-filled glovebox and the lithium metal electrodes were harvested and rinsed thoroughly with PC before analysis by SEM (LEO1550-FESEM). The only exception to this approach was for the electrode analysis aimed at characterizing the morphology and distribution of the lithium salt additives in the SEI, in which case the PC wash step was not employed.

Contact angles were measured at room temperature using a Ramé-hart, Inc. Model 100-00-115 goniometer. The lithium foil was placed in a transparent home-built environmental chamber with a rubber seal on the top. A single drop of the test liquid was placed on the substrate using a microlitre syringe through the seal. The contact angle was determined six times at different positions and the average values are reported. XPS (Surface Science Instruments, SSX-100) was used to characterize the surface chemistry of the lithium anode, with a scan range from 0 to 800 eV and high-resolution scanning near fluorine and lithium peaks. Ion sputtering using an inert gas ion gun was used to obtain chemical depth profiles down to 144 nm with a resolution of 12 nm.

Received 29 January 2014; accepted 23 June 2014;
published online 10 August 2014

References

1. Armand, M. & Tarascon, J-M. Building better batteries. *Nature* **451,** 652–657 (2008).
2. Yang, P. & Tarascon, J-M. Towards systems materials engineering. *Nature Mater.* **11,** 560–563 (2012).
3. Xu, K. Nonaqueous liquid electrolytes for lithium-based rechargeable batteries. *Chem. Rev.* **104,** 4303–4417 (2004).
4. Kang, B. & Ceder, G. Battery materials for ultrafast charging and discharging. *Nature* **458,** 190–193 (2009).
5. Morcrette, M. *et al.* A reversible copper extrusion-insertion electrode for rechargeable Li batteries. *Nature Mater.* **2,** 755–761 (2003).
6. Aricò, A. S., Bruce, P., Scrosati, B., Tarascon, J-M. & Schalkwijk, W. V. Nanostructured materials for advanced energy conversion and storage devices. *Nature Mater.* **4,** 366–377 (2005).
7. Whittingham, M. S. Materials challenges facing electrical energy storage. *Mater. Res. Bull.* **33,** 411–419 (2008).
8. Bruce, P. G., Freunberger, S. A., Hardwick, L. J. & Tarascon, J-M. Li–O_2 and Li–S batteries with high energy storage. *Nature Mater.* **11,** 19–29 (2012).
9. Jayaprakash, N., Shen, J., Moganty, S. S., Corona, A. & Archer, L. A. Porous hollow carbon@sulfur composites for high-power lithium–sulfur batteries. *Angew. Chem. Int. Ed.* **50,** 5904–5908 (2011).

10. Tarascon, J-M. & Armand, M. Issues and challenges facing rechargeable lithium batteries. *Nature* **414,** 359–367 (2001).
11. Bhattacharyya, R. *et al. In situ* NMR observation of the formation of metallic lithium microstructures in lithium batteries. *Nature Mater.* **9,** 504–510 (2010).
12. Lu, Y., Korf, K., Kambe, Y., Tu, Z. & Archer, L. A. Ionic-liquid–nanoparticle hybrid electrolytes: Applications in lithium metal batteries. *Angew. Chem. Int. Ed.* **53,** 488–492 (2014).
13. Lu, Y., Das, S. K., Moganty, S. S. & Archer, L. A. Ionic liquid–nanoparticle hybrid electrolytes and their application in secondary lithium-metal batteries. *Adv. Mater.* **24,** 4430–4435 (2012).
14. Tu, Z., Kambe, Y., Lu, Y. & Archer, L. A. Nanoporous polymer-ceramic composite electrolytes for lithium metal batteries. *Adv. Energy Mater.* **4,** 1300654 (2014).
15. Schaefer, J. L., Yanga, D. A. & Archer, L. A. High lithium transference number electrolytes via creation of 3-dimensional, charged, nanoporous networks from dense functionalized nanoparticle composites. *Chem. Mater.* **25,** 834–839 (2013).
16. Moganty, S. S. *et al.* Ionic liquid-tethered nanoparticle suspensions: A novel class of ionogels. *Chem. Mater.* **24,** 1386–1392 (2012).
17. Moganty, S. S., Jayaprakash, N., Nugent, J. L., Shen, J. & Archer, L. A. Ionic-liquid-tethered nanoparticles: Hybrid electrolytes. *Angew. Chem. Int. Ed.* **49,** 9158–9161 (2010).
18. Stone, G. M. *et al.* Resolution of the modulus versus adhesion dilemma in solid polymer electrolytes for rechargeable lithium metal batteries. *J. Electrochem. Soc.* **159,** A222–A227 (2012).
19. Monroe, C. & Newman, J. The impact of elastic deformation on deposition kinetics at lithium/polymer interfaces. *J. Electrochem. Soc.* **152,** A396–A404 (2005).
20. Nugent, J. L., Moganty, S. S. & Archer, L. A. Nanoscale organic hybrid electrolytes. *Adv. Mater.* **22,** 3677–3680 (2010).
21. Croce, F., Appetecchi, G. B., Persi, L. & Scrosati, B. Nanocomposite polymer electrolytes for lithium batteries. *Nature* **394,** 456–458 (1998).
22. Ding, F. *et al.* Dendrite-free lithium deposition via self-healing electrostatic shield mechanism. *J. Am. Chem. Soc.* **135,** 4450–4456 (2013).
23. Chazalviel, J-N. Electrochemical aspects of the generation of ramified metallic electrodeposits. *Phys. Rev. A* **42,** 7355–7367 (1990).
24. Rosso, M., Gobron, T., Brissot, C., Chazalviel, J-N. & Lascaud, S. Onset of dendritic growth in lithium/polymer cells. *J. Power Sources* **97–98,** 804–806 (2001).
25. Brissot, C., Rosso, M., Chazalviel, J-N. & Lascaud, S. Dendritic growth mechanisms in lithium/polymer cells. *J. Power Sources* **81–82,** 925–929 (1999).
26. De Jonghe, L. C., Feldman, L. & Millett, P. Some geometrical aspects of breakdown of sodium beta alumina. *Mater. Res. Bull.* **14,** 589–595 (1979).
27. Ansell, R. The chemical and electrochemical stability of beta-alumina. *J. Mater. Sci.* **21,** 365–379 (1986).
28. Aurbach, D. *et al.* Prototype systems for rechargeable magnesium batteries. *Nature* **407,** 724–727 (2000).
29. Ling, C., Banerjee, D. & Matsui, M. Study of the electrochemical deposition of Mg in the atomic level: Why it prefers the non-dendritic morphology. *Electrochim. Acta* **76,** 270–274 (2012).
30. Gunceler, D., Letchworth-Weaver, K., Sundararaman, R., Schwarz, K. A. & Arias, T. A. The importance of nonlinear fluid response in joint density-functional theory studies of battery systems. *Model. Simul. Mater. Sci. Eng.* **21,** 074005 (2013).
31. Gunceler, D., Schwarz, K. A., Sundararaman, R., Letchworth-Weaver, K. & Arias, T. A. *16th International Workshop on Computation Physics and Materials Science: Total Energy and Force Methods* (International Centre for Theoretical Physics, 2012).
32. Khurana, R., Schaefer, J. L., Archer, L. A. & Coates, G. W. Suppression of lithium dendrite growth using cross-linked polyethylene/polyethylene oxide electrolytes: A new approach for practical lithium-metal polymer batteries. *J. Am. Chem. Soc.* **136,** 7395–7402 (2014).
33. Jones, J., Anouti, M., Caillon-Caravanier, M., Willmann, P. & Lemordant, D. Lithium fluoride dissolution equilibria in cyclic alkylcarbonates and water. *J. Mol. Liq.* **153,** 146–152 (2010).
34. Tikekar, M. D., Archer, L. A. & Koch, D. L. Stability analysis of electrodeposition across a structured electrolyte with immobilized anions. *J. Electrochem. Soc.* **161,** A847–A855 (2014).
35. Ensling, D., Stjerndahl, M., Nyt'en, A., Gustafsson, T. & Thomas, J. O. A comparative XPS surface study of Li_2FeSiO_4/C cycled with LiTFSI- and LiPF6-based electrolytes. *J. Mater. Chem.* **19,** 82–88 (2009).
36. Wagner, C., Riggs, W., Davis, L., Moulder, J. & Muilenberg, G. *Handbook of X-ray Photoelectron Spectroscopy* (Perkin-Elmer, 1979).
37. Sotomura, T., Adachi, K., Taguchi, M., Tatsuma, T. & Oyama, N. Developing stable, low impedance interface between metallic lithium anode and polyacrylonitrile-based polymer gel electrolyte by preliminary voltage cycling. *J. Power Sources* **81,** 192–199 (1999).
38. Brousse, T. *et al.* All oxide solid-state lithium-ion cells. *J. Power Sources* **68,** 412–415 (1997).
39. Nakahara, K., Nakajima, R., Matsushima, T. & Majima, H. Preparation of particulate $Li_4Ti_5O_{12}$ having excellent characteristics as an electrode active material for power storage cells. *J. Power Sources* **117,** 131–136 (2003).
40. Lu, Y., Moganty, S. S., Schaefer, J. L. & Archer, L. A. Ionic liquid–nanoparticle hybrid electrolytes. *J. Mater. Chem.* **22,** 4066–4072 (2012).

Acknowledgements

This material is based on work supported as part of the Energy Materials Center at Cornell, an Energy Frontier Research Center funded by the US Department of Energy, Office of Science, Office of Basic Energy Sciences under Award Number DESC0001086. This work made use of the electrochemical characterization facilities of the KAUST-CU Center for Energy and Sustainability, which is supported by the King Abdullah University of Science and Technology (KAUST) through Award number KUS-C1-018-02. Y.L. thanks J. Jiang and C. Ober in the department of Material Science & Engineering at Cornell University for help with contact angle measurements. The thick LTO electrodes were produced at the US Department of Energy's (DOE) Cell Fabrication Facility, Argonne National Laboratory. The Cell Fabrication Facility is fully supported by the DOE Vehicle Technologies Program (VTP) within the core funding of the Applied Battery Research (ABR) for Transportation Program.

Author contributions

Y.L. and L.A.A. conceived the experiments reported in the manuscript. Y.L. performed all studies of the liquid electrolytes. These results are presented in Figs 1a, 2a–c, 3, 4 and 6. Z.T. performed experiments in which liquid electrolytes are infused in nanoporous alumina. These results are reported in Figs 1b and 2d. Y.L. and Z.T. performed the SEM and EDX analyses (Figs 2e–g and 5). Z.T. carried out the XPS analysis in the Supplementary Information. Y.L. and L.A.A. wrote the paper.

Additional information

Supplementary information is available in the online version of the paper. Reprints and permissions information is available online at www.nature.com/reprints. Correspondence and requests for materials should be addressed to L.A.A.

Competing financial interests

The authors declare no competing financial interests.